ADVANCED MATERIALS
www.advmat.de

Imperceptible Epidermal–Iontronic Interface for Wearable Sensing

*Zijie Zhu, Ruya Li, and Tingrui Pan**

Recent development of epidermal electronics provides an enabling means to continuous monitoring of physiological signals and close tracking of physical activities without affecting quality of life. Such devices require high sensitivity for low-magnitude signal detection, noise reduction for motion artifacts, imperceptible wearability with long-term comfortableness, and low-cost production for scalable manufacturing. However, the existing epidermal pressure sensing devices, usually involving complex multilayer structures, have not fully addressed the aforementioned challenges. Here, the first epidermal–iontronic interface (EII) is successfully introduced incorporating both single-sided iontronic devices and the skin itself as the pressure sensing architectures, allowing an ultrathin, flexible, and imperceptible packaging with conformal epidermal contact. Notably, utilizing skin as part of the EII sensor, high pressure sensitivity and high signal-to-noise ratios are achieved, along with ultralow motion artifacts for both internal (body) and external (environmental) mechanical stimuli. Monitoring of various vital signals, such as blood pressure waveforms, respiration waveforms, muscle activities and artificial tactile sensation, is successfully demonstrated, implicating a broad applicability of the EII devices for emerging wearable applications.

Epidermal electronics, built upon extremely flexible and ultrathin functional materials, enables brand-new modalities to track various body biosignals via an intimate body contact through the skin.[1–8] Compared to the traditional silicon-based counterparts, its conformal attachment onto skin significantly reduces motion artifacts and associated noises.[9–13] In particular, mechanical sensing, mimicking our skin mechanoreception in an epidermal packaging, has attracted considerable attention in both academia and industries, which can be potentially extended to a wide range of emerging high-impact applications, such as body vital signal monitoring,[14,15] wearable rehabilitation therapy,[16,17] and human–machine interfaces.[18] Several sensing mechanisms, derived from the solid-state sensing technologies, have been explored and applied toward the epidermal mechanical sensing, including resistive, capacitive, and piezoelectric detection principles. Among those, the resistive sensors, also known as force sensitive resistor, are most commonly used with an array of newly introduced functional material options, for example, graphene-polyurethane sponge,[19] seaurchin-shaped metal nanoparticles within polyurethane elastomer,[20] AuNWs-impregnated tissue paper,[21] and carbonized silk nanofiber.[22] Recently, ionic materials have also been used as conductive agents to construct flexible and stretchable resistive sensors for wearable motion detection.[23,24] These elastic devices directly convert external mechanical deformation into the changes of electrical resistance with a simple device layout and low cost. To further enhance the mechanical sensitivity, elastic and conductive microstructures, e.g., micropillars, microdomes, and micropyramids, have been incorporated in the device architecture, along with a group of new conductive coating materials, including graphene,[25] single-wall carbon nanotubes,[26] and poly(3,4-ethylenedioxythiophene):poly(styrenesulfonate) (PEDOT:PSS)/polyurethane dispersion (PUD).[27] However, the resistive nature of these materials leads to their intrinsically high sensitivity to any thermal noises and variations from both human body and external environment.[28] Alternatively, piezoelectric materials, e.g., zinc oxide nanowires[29] and lead zirconate titanate ($PbZr_{0.52}Ti_{0.48}O_3$),[30] have also been utilized for epidermal mechanical sensing with excellent sensitivity and high spatial resolution. Unfortunately, they can only be operated under dynamic sensing modes due to the intrinsic charge leakage, and the sensing accuracy can suffer from the complicated microfabrication and material processing, in addition to their high production cost.[31] Moreover, devices based on the capacitive sensing principle have shown several advantages over their counterparts in terms of temperature immunity, low power consumption, and simple device architecture,[9,32] but limited capacitive readouts in typical pF ranges are highly subject to parasitic noises from body and environmental sources (which can be up to hundreds of times of the signals).[33] Therefore, new sensing modalities with high device sensitivity and high noise immunity along with conformal packaging and attachment to human body are still highly sought-after for fast-growing applications in wearable and epidermal sensing.

Recent development of ionic materials and iontronic sensing mechanism provides an attractive alternative to the existing

Z. Zhu, Dr. R. Li, Prof. T. Pan
Micro-Nano Innovations (MiNI) Laboratory
Department of Biomedical Engineering
University of California
Davis, CA 95616, USA
E-mail: tingrui@ucdavis.edu
Z. Zhu
Department of Electrical and Computer Engineering
University of California
Davis, CA 95616, USA

DOI: 10.1002/adma.201705122

technologies, by providing ultrahigh unit-area capacitance, remarkable signal-to-noise ratio, excellent mechanical flexibility, and distinct optical transparency.[34] For instance, Suo's group has reported a highly stretchable, transparent, and biocompatible ionic hydrogel-based capacitive sensor, which can detect external pressure as low as 1 kPa.[35] Our group has formerly introduced iontronic microdroplet sensors, which can be utilized as both discrete and arrayed pressure-sensing elements to achieve ultrahigh device sensitivities (as high as 0.43 nF kPa^{-1}).[15,36,37] Further investigations on pressure-sensitive iontronic materials have led newly enabling features, including broad sensing ranges, e.g., from a few pascals up to 50 kPa,[38] and extended material selection choices, e.g., completely fabric-made devices for truly continuous wearability.[8] Notably, distinct from the traditional parallel-plate capacitive sensors, the iontronic devices, made from ionic materials (e.g., ionic liquids, ionic gels, or ionic nanofibers), primarily utilizes a remarkably electronic–ionic capacitive interface, known as an electric double layer (EDL), established at a sub-nanoscale material contact, which is subject to change under external mechanical stimuli. This stress/pressure-induced capacitive change can be significant at the nanoscopic EDL interface (which can be at least three orders of magnitude higher than that of the parallel-plate counterparts)[14,15,39] and can substantially overcome the long-standing parasitic noise issues.[8] Up-to-date, the iontronic sensors have not yet been demonstrated its conversion into an epidermal electronic format with an intimate skin contact due to both electronic designs and material/packaging challenges.

In this communication, we have presented the first skin-interfaced iontronic pressure-sensing architecture for wearable sensing, based on the emerging iontronic detection principle in an easy-to-apply imperceptible and ultrathin (1.9 μm) packaging. In particular, the brand-new mechanical sensing architecture built upon the epidermal–iontronic interface (EII) has been implemented in these iontronic sensors with a single-sided electrode configuration, which incorporates the conductive human skin as an electric return and the ground of the sensing device. Markedly, it is the first time that the direct epidermal contact has been demonstrated as a unique iontronic sensing interface. As a result, this type of device architecture enables to acquire both internal (body) and external (environmental) mechanical stimuli with high sensitivities and high signal-to-noise ratios. In such a case, the electrical layouts can become extremely simple and the device can stay highly adaptive for extended wearability. Moreover, by choosing a Nafion-derived material as the biocompatible ionic electrode, EII devices can be directly mounted and placed into a physical contact with human skin without causing any safety concern.[40,41] Resulted from the inherent interfacial property of the iontronic materials, the ionic film, upon contact, can immediately form an ultrahigh unit-area capacitance (55.6 nF cm^{-2}) between itself and human skin, in addition to its optical transparency (85%). By introducing a reference unit, variations of the unit-area capacitance, from both temperature and humidity influences, can be largely reduced (less than 5%). Furthermore, additional device characterization studies have been carried out and reported in the following sections, including the pressure sensitivity (up to 5 nF kPa^{-1}), the time response (in a sub-millisecond range), the extended mechanical repeatability/reliability (>10 000), and the device performance on both planar and curved surfaces. In the last part, we have successfully demonstrated the capacity of the EII device. This includes the attachment of this type of devices onto different parts of human body, from which both tracking of internal body physiological signals, e.g., blood pressure pulsations (temple, carotid, radial, and dorsalis pedis), respiration rates (abdomen), and muscle activities (upper arm, chest, and thigh), and artificial tactile sensing of external loads (hand) have been exhibited in a conformable package.

Figure 1a illustrates the human skin-incorporated device architecture, the EII, of the iontronic sensors. From the top to bottom, it is comprised of only a supporting flexible substrate, an ionic electrode layer, and an adhesive layer, while utilizing the intrinsically conductive skin layer as an electric return and the ground. Specifically, under external mechanical loads, the ionic electrode is deformed and forms an electronic–ionic contact with skin, which triggers establishment of the iontronic capacitance, as shown in Figure 1b. As the external load increases, the epidermal–electronic contact area would gradually rise, which can be detected electronically by measuring the appreciable change in the capacitive value. The circuit diagram in Figure 1c illustrates the equivalent circuit model for the EII device, in which one fixed capacitor (C_{EI}) indicates the interfacial capacitance between the electrode and ionic layers, whereas the variable one (C_{EE}) represents the EDL capacitance altering with the area of the electronic–epidermal contact. It is worth noting that the unit-area capacitance of the EDL is in the range of nF cm^{-2}, which is substantially greater than that of the ubiquitous human body capacitance and other parasitic capacitive noises.[33,42] Figure 1d,e exhibits a microfabricated array of EII sensors with various dimensions and 14-unit sensing arrays amounted onto both a human hand and a robotic hand. In brief, the novel single-sided ionic device architecture would allow the sensors to be simply fabricated (a straightforward three-layer structure), while highly adaptive to any conductive surfaces (e.g., metals, conductive polymers, and skins) or even nonconductive surfaces (e.g., artificial skins), as long as a thin conductive coating can be applied.

As the core of the EII device, we have selected Nafion, a perfluorosulfonate linear ion-exchange polymer, as the ionic material, due to its excellent ionic conductivity, mechanical strength, film forming ability, optical transparency, and biocompatibility.[43] As mentioned previously, the EDL established between the epidermal and the iontronic material serves as a key component to enable the ultrahigh interfacial capacitance and device sensitivity. In our case, the stratum corneum, the outermost layer of the epidermis and composed of dead cells, has in direct contact with the flexible iontronic electrode, forming an EDL at the interface. Moreover, it is known that both epidermal temperature and hydration level are highly dependent on body location and environmental moisture content.[44,45] In such a case, the EII is under heavy influences of skin conditions, of which both temperature and hydration levels can largely affect the unit-area capacitance of the EDL and change the device responses.

Here, we have fully investigated into characterization of the EII, including frequency responses of the EDL of the Nafion-based

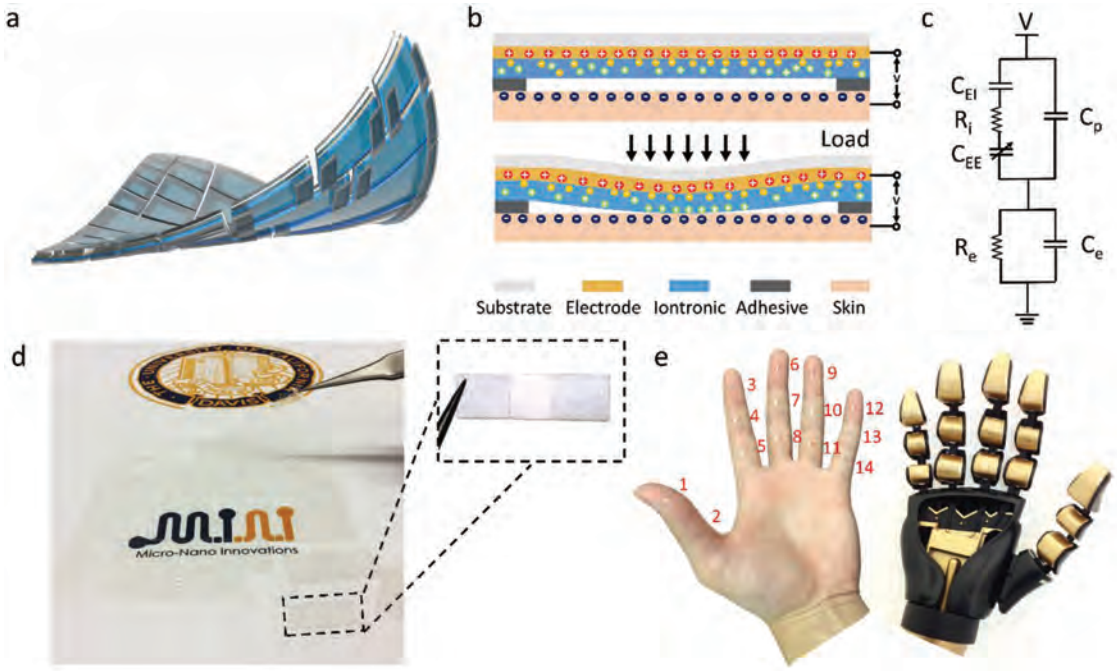

Figure 1. a) Perspective view and b) cross-sectional view of the EII devices, consisting a supporting substrate, an ionic electrode layer, and an adhesive layer, along with c) the equivalent electrical circuit model. Photographs of d) a microfabricated array of EII sensors with various dimensions and e) a 14-unit sensing array amounted onto both a human hand and a robotic hand.

iontronic electrode in contact with different parts of human skin (e.g., finger, feet, head, neck, wrist, and abdomen), as well as EDL responses to multiple environmental variables (including humidity and temperature). As summarized in **Figure 2**a, the unit-area capacitance decreases with the rise of electrical acquisition frequency. In particular, the two finger–iontronic interfaces, with or without conductive gel applied, exhibit a relatively larger unit-area EDL capacitance, the higher one of which reduces from 55.6 to 20.1 nF cm^{-2}, as the frequency increases from 20 Hz to 1 kHz. While, on other parts of human skin, the induced EDLs follow a similar trend but show a smaller capacitive value. A likely reason can attribute to the fact that lower skin moisture level presents in a thinner epidermis layer, leading to a poor ionic environment over the skin surface.[46] Moreover, the inset plot of Figure 2a illustrates that the gold–iontronic interface possesses a larger EDL capacitance than that of the indium tin oxide (ITO)–iontronic interface, which may be contributed by a higher surface charge density or a reduced Debye length presented.[47,48] Specifically, the unit-area capacitance of the diffusion layer, according to the classic Gouy–Chapman–Stern Model,[49] increases in proportion to the Debye length of electrolytes. And the Debye length depends only on the properties of the electrolyte (e.g., ionic species and concentrations) and is independent of the interface and its electrical state.[50] Figure 2b summarizes the unit-area capacitance under the influence of environmental humidity and temperature. As can been seen, the measured capacitances show an increase from 20.3 to 103.2 nF cm^{-2} at 20 Hz, as the humidity level elevates from 50% to 90% at a constant temperature (of 20 °C). Whereas, an increase from 20.3 to 27.1 nF cm^{-2} has been observed, as the temperature rises from 20 to 50 °C at a constant humidity level (of 50%). This humidity and temperature induced variations of the EDL capacitance may attribute to the changes of ion transfer capability of the Nafion layer according to the literature.[51] In order to eliminate the fluctuations of the unit-area capacitance caused by environmental uncertainties, an adjacent reference unit has been introduced, which is placed beside the sensing unit to track the change of the unit-area capacitance, analogous to a typical Wheatstone bridge circuitry (Figure S1, Supporting Information). As plotted in Figure 2c, the relative capacitive change (C/C_{ref}) can be monitored under this configuration instead, illustrating only a marginal influence (less than 5%) by both humidity and thermal variations from body and environments.

Distinct from the traditional pressure sensors that typically employ complex multilayer structures, the EII sensors only involve a single-sided electrode and the skin itself in the device configuration, allowing to be easily applied onto the body surface in an ultrathin and imperceptible packaging. Particularly, an ultrathin EII pressure sensor with a substrate of 1.9 μm in thickness has been achieved with full functionality for extended wearability and imperceptibility (Figure S2, Supporting Information). Due to the ultrathin construction (of 5 g m^{-2} in weight), these devices can be easily floated onto soap bubbles (Figure 2e). Its excellent flexibility has been demonstrated in Figure S3 in the Supporting Information, where the ultrathin EII sensors can be wrapped around capillary tubes with radii down to 180 μm. Utilizing a commercial thin skin adhesive (e.g., temporary tattoo paper), we can apply the conformal attachment of the ultrathin EII device onto human skin (Figure 2f). Such a thin construction and conformal attachment allow the device to be stretched and compressed with the skin reversibly and unnoticeably. We have also investigated the EII sensor performances under different strain conditions (Figure S4,

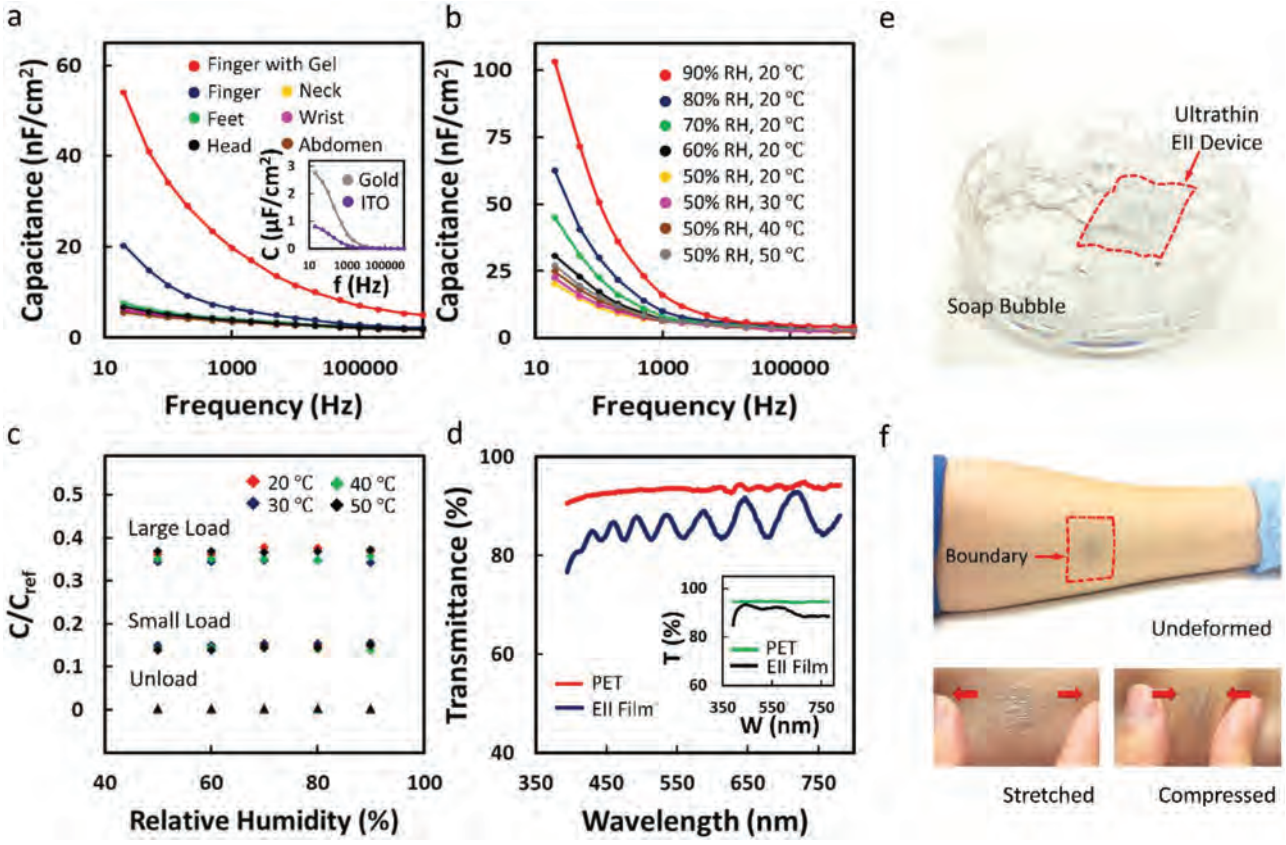

Figure 2. EII characterizations of: a) the unit-area EDL capacitances of epidermal–iontronic contact in various positions; b) the influence of humidity and temperature on the unit-area EDL capacitance; c) the relative capacitive changes of the sensing unit to the reference unit under large (10 kPa) and small (3 kPa) loads, with temperature ranging from 20 to 50 °C and humidity ranging from 50 to 90 RH%. d) Characterization of the optical transmittance of the EII devices. Photographs of ultrathin EII devices e) floating on soap bubbles and f) attaching onto human skin: undeformed, stretched, and compressed, illustrating its high flexibility and wearability.

Supporting Information), in which marginal variations in capacitive readouts (less than 6%) have been observed. Figure 2d summarizes the results of the optical transmittances of an EII film with a substrate layer (polyethylene terephthalate, PET) (of 75 μm in thickness), an electrode layer (ITO), and an ionic layer (Nafion), within a visible light spectrum (380–780 nm). Importantly, the EII film remains a high transparency (>80%) and the periodic variations in the optical spectrum, caused by the constructive and destructive interferences, imply a flat coating of the ionic layer.[52] The insert plot shows the optical transmittance of an ultrathin EII film (>85%) with an ultrathin substrate layer (PET) (of 1.9 μm in thickness), an electrode layer (PEDOT:PSS), and an ionic layer (Nafion).

According to the classic mechanical deformation theory,[53] the relationship between the uniformly loaded external pressure (P) and the induced rectangular membrane deformation can be modelled as two oppositely clamped edges with the other two free ones. Here, we have also assumed that when the contact has been made between the epidermal and ionic surfaces, the equivalent membrane can be considered as a membrane with a reduced length, which has been validated by Ko's group.[54–56] Thus, the expression to calculate the induced EDL capacitance (C) can be derived as given below (the detailed derivations can be found in the Supporting Information)

$$C = C_0 l\left(l - \sqrt[4]{\frac{hEt^3}{0.03\left(1-\nu^2\right)P}}\right) \tag{1}$$

where l and t stand for the length and the thickness of the sensing membrane, respectively, while E represents Young's modulus and ν is its Poisson ratio. h is considered as the initial separation distance between the ionic electrode and the skin surface, which is equal to the thickness of the adhesive layer under no load condition.

In order to fully evaluate the performance of the EII sensors, we have implemented a series of mechanical characterization procedures, including sensitivity, mechanical response, repeatability, and surface curvature effects. It is considered that continuous pressure loading is more applicable scenarios in epidermal pressure sensing (e.g., tactile sensation, blood pressure pulsation, and body motion tracking), given the miniature sensing area of the ionic EII devices.[57] Therefore, we have applied a uniform pressure on the EII sensors in mechanical calibrations (Figure S5, Supporting Information). **Figure 3**a–c summarizes the characterization results from the device sensitivity measurements, where the changes of the interfacial capacitance of the sensing devices vary with the uniformly loaded external pressure over the rectangular sensing membrane.

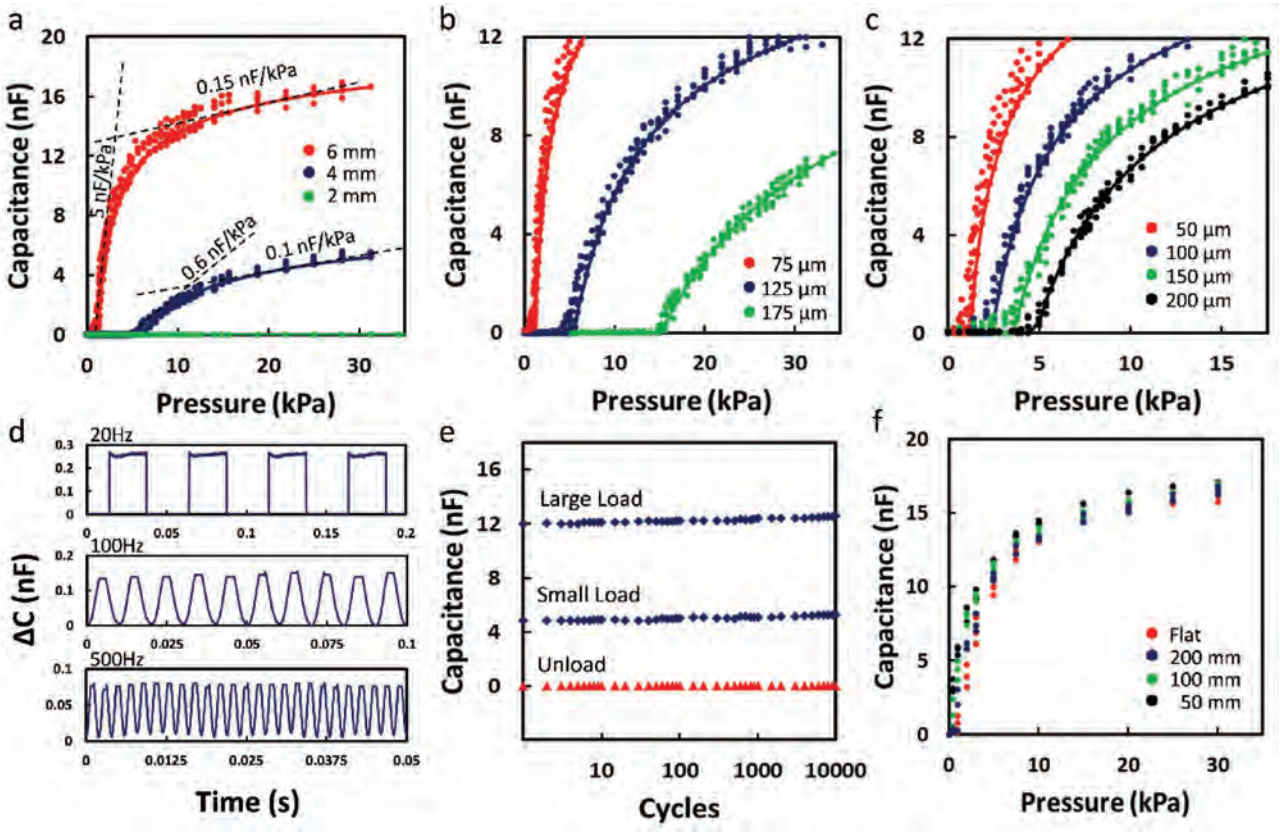

Figure 3. Experimental (dots) and theoretical (solid lines) investigations of the device sensitivity and threshold pressure: a) with different lengths of the sensing area, at a constant sensing membrane thickness of 75 μm and adhesive thickness of 50 μm; b) with different sensing membrane thicknesses, at a constant length of the sensing area of 6 mm and adhesive thickness of 50 μm; c) with different adhesive thicknesses, at a constant length of the sensing area of 6 mm and sensing membrane thickness of 75 μm. d) Time-resolved mechanical response of the EII sensor under cyclic external loads with the frequency of 20, 100, and 500 Hz. e) Capacitive changes of the EII sensor under a large (10 kPa) and a small (3 kPa) cyclic external load (10 000), respectively. f) Investigation of the surface curvature effects, with sensors on both flat surface and curved surfaces.

In particular, four regions (noncontact region, transition region, linear response region, and saturation region) have been observed and recorded, which is in a close agreement with the previous publications.[15,54–56] We have selected several characteristic geometrical parameters in the EII sensor design to control and fine-tune device sensitivity, based on the previously presented model. These include the length of the sensing area, the thickness of the deforming substrate, and the height of the adhesive layer. As can be seen, the experimental data were collected and plotted (as dots) in comparison with the theoretical predictions generated by the model (in lines). We first look into the influence of the length of the sensing membrane, while keeping constant its thickness at 75 μm and the separating distance of 50 μm from the substrate (Figure 3a). In this case, the sensor with a larger sensing area (of 6 mm in length) shows a significantly higher device sensitivity (in red dots), i.e., 5 nF kPa^{-1} in a low-pressure range (<5 kPa) and 0.15 nF kPa^{-1} in a high-pressure range (10–30 kPa). In addition, the size of the sensing membrane also determines the threshold pressure for mechanical measurements, upon which the initial physical contact forms between the ionic membrane and the substrate. For the sensor with the smallest sensing area (of 2 mm in length), it requires a substantial threshold pressure (95 kPa) to start the initial contact. Moreover, the membrane thickness also plays a role in the device sensitivity and the threshold pressure, according to the model. As expected, the device sensitivity decreases from 5 to 0.65 nF kPa^{-1}, and the threshold pressure rises from less than 1 to 15 kPa, by adjusting the membrane thickness from 75 to 175 μm, given a constant sensing membrane of 6 mm in length and the separation height of 50 μm (Figure 3b). Furthermore, the sensors with a smaller gap (of 50 μm), controlled by the thickness of the adhesive layer, exhibit a higher sensitivity (5 nF kPa^{-1}) and a lower threshold pressure (0.8 kPa) (Figure 3c). This is mainly due to smaller deformations to establish contacts between the ionic film and the substrate under the same external pressure.

One of the key advantages is the rapid response for the EII film based mechanical sensing.[15] To characterize the device mechanical responses, time-resolved experiments have been conducted on EII sensors with a sensing membrane of 6 mm in length and 75 μm in thickness, and 50 μm in spacing (the circuit diagram has been shown in Figure S6, Supporting Information). As plotted in Figure 3d, the measured capacitive changes directly follow the controlling signals to the piezoelectric actuator with a negligible time delay (less than a millisecond). This fast-responding behavior has been extended to a frequency up to 500 Hz. The rapid response of the EII sensors mainly attributes to the designs of the sensing structure

(i.e., the parallel-plate configuration) and the material properties of the membrane (e.g., nonelasticity and relatively high Young's modulus).[15,58] Moreover, the rapid polarization of the Nafion-ionic film also ensures the fast response electrically.[43] In addition, extended cyclic tests have been implemented (Figure 3e). Both a high (i.e., 10 kPa) and low mechanical load (i.e., 3 kPa) have been applied to the EII sensors at 100 Hz, respectively. After 10 000 cyclic testing, the drift of the sensor is less than 5% for both of them, which exhibits its high reliability and repeatability. Furthermore, the surface curvature effects have also been investigated, in which the sensors are bent outward symmetrically. As shown in Figure 3f, the capacitive changes of the sensors have been measured as the external pressure rising from 0 to 30 kPa, under different radii of curvatures, ranging from 50 mm to infinite (flat). A minimal variation (less than 5%) has been observed on both flat and curved surfaces, indicating a wide applicability of the EII devices to curved geometry (e.g., various body contours).

After establishing the EII sensors onto different parts of human skin, we have utilized and demonstrated the sensors to track mechanical signals from both inside or outside of human body. It can be configured under various scenarios, e.g., pulse sensing, respiration tracking, muscle activity monitoring, and human hand pressure mapping, benefiting from its novel one-side architecture, high pressure-sensitivity, rapid time response, and immunity to noises. Considering the requirements for various use cases, the substrates with different thicknesses have been selected to satisfy pressure sensitivity and sensing range in the corresponding EII devices. Specifically, to detect internal body signals (**Figure 4**a–h), a PET film of 75 µm in thickness has been utilized as the substrate for the EII sensors. And to map hand gripping pressure (Figure 4i), an ultrathin PET film of 1.9 µm in thickness has been used.

Figure 4a–d summarizes the real-time blood pressure waveforms recorded from a healthy adult volunteer (27 year old) above temporal artery, carotid artery, radial artery, and dorsalis pedis artery, respectively. Importantly, all of these physiological data may have great clinical significance in modern medical diagnosis.[59–62] Although temporal pulses and dorsalis pedis pulses are typically more difficult to be palpated even by experienced clinicians, in our case, the pulse waveforms have been reliably obtained for all these body positions, upon an appropriate external pressure applied. In addition, the blood pressure waveforms of radial artery provide more detailed features, including systolic peak, reflected systolic peak, and diastolic peak, as shown in Figure S7 in the Supporting Information, which can be used to detect additional hemodynamic parameters, such as pulse wave velocity and arterial stiffness, for non-invasive clinical assessments.[63]

Respiration monitoring is another important component of wearable electronics for both medical diagnosis and consumer applications.[64,65] To this end, we have attached the EII sensors onto the skin of the abdomen. Different from conventional breath sensing devices that measure either the expansion of peripheral length of the chest or the change of blood oxygen level,[66] the EII sensors can be used to monitor the breath patterns by detecting pressure variations generated locally from human body during the respiratory cycles, which can eliminate a significant portion of motion artifacts. Figure 4e shows the results of recorded breath signals with four distinctive breath modes, i.e., normal (≈0.4 Hz), deep (≈0.2 Hz), holding, and rapid (≈1 Hz).

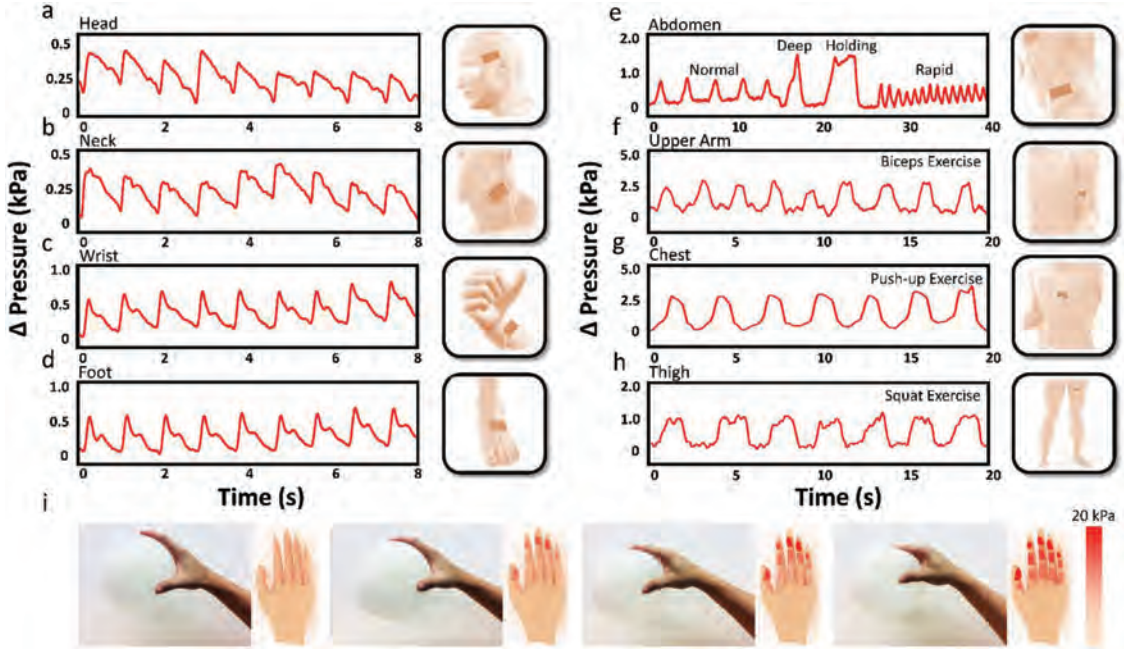

Figure 4. Time-resolved pulse waveform recorded by attaching the EII sensors onto the skins above a) temporal artery, b) carotid artery, c) radial artery, and d) dorsalis pedis artery. e) Time-resolved breath signals recorded by attaching the EII sensor onto the abdomen skin. Time-resolved muscle activities recorded by attaching the EII sensors onto f) upper arm, g) chest, and h) thigh. i) Pressure distribution of human hand while pressing a soft balloon recorded by 14 ultrathin EII sensors on human hand, i.e., two on the thumb and three on each of the others.

In principle, specific muscular activities are directly related to the changes of its longitudinal contraction or elongation and associated expansion of the cross-sectional area.[67] Based on this principle, we have shown the capacity of the EII sensors to precisely track minute changes of the local skin interfacial pressure (Figure S8, Supporting Information). The EII sensors have been attached onto various parts of human body, including upper arm, chest, and thigh, respectively, and the corresponding pressure variations have been measured continuously. Figure 4f demonstrates the pressure changes of the sensor directly attached above the biceps muscle, as a healthy volunteer lifts up a dumbbell periodically in biceps exercise. The contraction of the biceps muscle generates a significant transverse pressure that transmits through the skin and applies onto the EII sensor. Alternating between the contraction and elongation states, a repetitive pressure change of 2.5 kPa has been observed and recorded, which closely matches with the muscular movements in the arm. Similarly, the EII sensor attached onto the chest of the volunteer measures the movement of the pectoralis muscle in push-up exercise, as shown in Figure 4g, which produces a normal pressure increase of 2.8 kPa from the muscular contraction. While, Figure 4h shows the physical activity of the rectus femoris muscle as the volunteer conducts squat exercise, of which an interfacial pressure variation of 1.0 kPa has been detected.

To explore the applicability of the EII sensors to artificial tactile sensing, we have attached 14 sensing units onto a human hand, one located in each finger phalange (Figure 1e), for whole-hand grip pressure analysis.[68] Figure 4i shows the results of gentle pressure variations on a human hand while pressing a soft balloon. As can be seen, a pressure gradient (≈2 kPa cm^{-1}) has been established along the fingers as the gripping force rises and reaches the maximum value at the fingertip, in which way the balloon can be held stably. A time-resolved grip pressure distribution is summarized in Figure S9 in the Supporting Information. Compared with existing commercial grip analyzers (e.g., Tekscan), EII sensors offer imperceptible and conformal packaging with ultrahigh sensitivity, significantly reduced motion artifacts, and extended wearability.[69]

In summary, we have first presented and characterized a highly sensitive, highly adaptive, noise-immune human-wearable interface, referred to as EII, in this communication, which incorporates conductive human skin as part of the device and utilizes a novel sensing mechanism of interfacial iontronic capacitance. The simple single-sided device architecture enables the EII devices to be applicable onto any flexible and curved surfaces with electrical conductance. This novel architecture also enables the wearable sensing devices with ultrahigh pressure sensitivity (of 5 nF kPa^{-1}), fast mechanical response (in sub-milliseconds), and long-term stability (>10 000). It is the first time that the direct epidermal–electrode contact has been demonstrated as a unique sensing interface, of which this architecture enables to acquire both internal (body) and external (environmental) mechanical stimuli. The utility of the EII sensing architecture for body signal acquisition has been fully demonstrated by cardiovascular pulse waveform detection, respiration rate monitoring, and muscular activity tracking, over multiple skin locations. For the external tactile responses, we have illustrated the capacity of EII devices to map grip pressure distribution by amounting the sensors over the hand. In brief, the new EII devices have shown great promises with outstanding electrical and mechanical properties along with long-term stability and repeatability, which can be highly attractive to emerging wearable and medical applications.

Experimental Section

Iontronic Film Preparation: Different thicknesses of PET substrate coated with indium-tin-oxide (ITO) (Mianyang Prochema Commercial Co.) were used as the electrode layer. An iontronic Nafion solution of 1 mL was prepared by mixing 500 µL Nafion solution (D2020, Ion Power Inc.) and 500 µL alcohol (AX0441, EMD). To prepare the ionic film, the Nafion solution was spin coated onto ITO substrates at 1000 rpm for 30 s (WS-400-6NPP, Laurell). As follow, the film was baked in an oven at 80 °C for 60 min. The preparation of the ultrathin ionic films followed the same procedure. The ultrathin PET substrates (thickness of 1.9 µm) (Shijiazhuang Dadao Packaging materials Co.) coated with PEDOT:PSS (Clevios PH 1000, Heraeus) were used as the electrode layer. The PET substrate was treated first with oxygen plasma for 1 min, and the PEDOT:PSS solution was spin coated at 5000 rpm for 30 s (WS-400-6NPP, Laurell). After baking at 120 °C on a hot plate in ambient air for 15 min, PEDOT:PSS coated PET films were immediately immersed in ethylene glycol bath for 15 min and then annealed for another 15 min at 120 °C.

Device Fabrication: To obtain desired geometrical shapes, a desktop CO_2 pulsed laser engraver (VersaLaser, Universal Laser) was used. The laser-trimmed iontronic film and double-sided tape (3M) were bonded together, forming a sheet of stick-on sensors with various sensing dimensions. In different applications, sensors with appropriate size were cut from the sheet using scissors, followed by electrical wire connection to one end of the electrode layer. The fabrication of the ultrathin EII devices followed the same procedure but using the temporary adhesive tattoo paper (Silhouette) as the adhesive layer. In addition, a transfer tape (Angel Crafts) mount the EII sensors onto different parts of human skin was utilized.

Measurement Setup: In EII characterizations, the unit-area interfacial capacitance was measured by an LCR meter (4284A, Agilent), of which the sweeping frequency was ranging from 20 Hz to 1 MHz. A humidity generator (7144, Air-O-Swiss) was used to generate various environmental moisture levels, which is monitored by a humidity sensor (HT110, PCE). And a heating pad was applied to increase operation temperature, which is tracked by an IR thermodetector (DT-8380, Riversong). To illustrate optical transmittance of the iontronic film, a microplate reader (Safire2, Tecan) was used with wavelength sweeping from 380 to 780 nm. To characterize the device sensitivity, the capacitive changes were measured by an LCR meter, under different uniform pressures provided by an air-filled bladder (PicoPress, MediCad) that was connected to and monitored by a digital manometer (840080, Sper Scientific). A computer-controlled moving stage (VT-80, PImicos) was used to precisely control the movement of the bladder. Mechanical response and repeatability were implemented by periodic loads driven by a piezoelectric actuator (T215-A4-303 (Y), Piezo Systems Inc.) with a square wave signal of 40 V from 20 to 500 Hz and the evolutions of the output signals were recorded by a custom readout circuit at a sampling frequency of 10 kHz. For characterization of the surface curvature effect, the EII sensors were attached onto convex surfaces with different radii of curvatures (50, 100, and 200 mm) using a double-sided tape. To avoid the initial deformation of the sensing layer, the transfer tape was first bonded to the precurved surfaces prior to the device packaging.

Supporting Information

Supporting Information is available from the Wiley Online Library or from the author.

Acknowledgements

Z.Z. and R.L. contributed equally to this work. This work was in part supported by the National Science Foundation (NSF) Award (ECCS-1307831) to T.P. The authors would like to thank Dr. Erkin Seker and Dr. Ning Pan for valuable suggestions for theoretical model calculations.

Conflict of Interest

The authors have been involved in several startup companies developing wearable technologies.

Keywords

epidermal electronics, epidermal–iontronic interfaces, iontronic sensing, pressure sensing

Received: September 7, 2017
Revised: November 12, 2017
Published online:

[1] D.-H. Kim, N. Lu, R. Ma, Y.-S. Kim, R.-H. Kim, S. Wang, J. Wu, S. M. Won, H. Tao, A. Islam, *Science* **2011**, *333*, 838.
[2] M. Kaltenbrunner, T. Sekitani, J. Reeder, T. Yokota, K. Kuribara, T. Tokuhara, M. Drack, R. Schwödiauer, I. Graz, S. Bauer-Gogonea, *Nature* **2013**, *499*, 458.
[3] M. L. Hammock, A. Chortos, B. C. K. Tee, J. B. H. Tok, Z. Bao, *Adv. Mater.* **2013**, *25*, 5997.
[4] J. W. Jeong, W. H. Yeo, A. Akhtar, J. J. Norton, Y. J. Kwack, S. Li, S. Y. Jung, Y. Su, W. Lee, J. Xia, *Adv. Mater.* **2013**, *25*, 6839.
[5] D. Son, J. Lee, S. Qiao, R. Ghaffari, J. Kim, J. E. Lee, C. Song, S. J. Kim, D. J. Lee, S. W. Jun, *Nat. Nanotechnol.* **2014**, *9*, 397.
[6] S. Yang, Y. C. Chen, L. Nicolini, P. Pasupathy, J. Sacks, B. Su, R. Yang, D. Sanchez, Y. F. Chang, P. Wang, *Adv. Mater.* **2015**, *27*, 6423.
[7] Z. Zhu, G. Yang, R. Li, T. Pan, *Microsys. Nanoeng.* **2017**, *3*, 17004.
[8] R. Li, Y. Si, Z. Zhu, Y. Guo, Y. Zhang, N. Pan, G. Sun, T. Pan, *Adv. Mater.* **2017**, *29*, 1700253.
[9] C. Pang, J. H. Koo, A. Nguyen, J. M. Caves, M. G. Kim, A. Chortos, K. Kim, P. J. Wang, J. B. H. Tok, Z. Bao, *Adv. Mater.* **2015**, *27*, 634.
[10] M. K. Choi, O. K. Park, C. Choi, S. Qiao, R. Ghaffari, J. Kim, D. J. Lee, M. Kim, W. Hyun, S. J. Kim, *Adv. Healthcare Mater.* **2016**, *5*, 80.
[11] D. M. Drotlef, M. Amjadi, M. Yunusa, M. Sitti, *Adv. Mater.* **2017**, *29*, 1701353.
[12] S. H. Jeong, S. Zhang, K. Hjort, J. Hilborn, Z. Wu, *Adv. Mater.* **2016**, *28*, 5830.
[13] Y. Park, J. Shim, S. Jeong, G. R. Yi, H. Chae, J. W. Bae, S. O. Kim, C. Pang, *Adv. Mater.* **2017**, *29*, 1606453.
[14] G. Schwartz, B. C. Tee, J. Mei, A. L. Appleton, D. H. Kim, H. Wang, Z. Bao, *Nat. Commun.* **2013**, *4*, 1859.
[15] B. Nie, R. Li, J. Cao, J. D. Brandt, T. Pan, *Adv. Mater.* **2015**, *27*, 6055.
[16] B. C.-K. Tee, A. Chortos, A. Berndt, A. K. Nguyen, A. Tom, A. McGuire, Z. C. Lin, K. Tien, W.-G. Bae, H. Wang, *Science* **2015**, *350*, 313.
[17] R. Li, B. Nie, C. Zhai, J. Cao, J. Pan, Y.-W. Chi, T. Pan, *Ann. Biomed. Eng.* **2016**, *44*, 2282.
[18] S. Jung, J. H. Kim, J. Kim, S. Choi, J. Lee, I. Park, T. Hyeon, D. H. Kim, *Adv. Mater.* **2014**, *26*, 4825.
[19] H. B. Yao, J. Ge, C. F. Wang, X. Wang, W. Hu, Z. J. Zheng, Y. Ni, S. H. Yu, *Adv. Mater.* **2013**, *25*, 6692.
[20] D. Lee, H. Lee, Y. Jeong, Y. Ahn, G. Nam, Y. Lee, *Adv. Mater.* **2016**, *28*, 9364.
[21] S. Gong, W. Schwalb, Y. Wang, Y. Chen, Y. Tang, J. Si, B. Shirinzadeh, W. Cheng, *Nat. Commun.* **2014**, *5*, 3132.
[22] Q. Wang, M. Jian, C. Wang, Y. Zhang, *Adv. Funct. Mater.* **2017**, *27*, 1605657.
[23] Y. Wang, S. Gong, S. J. Wang, G. P. Simon, W. Cheng, *Mater. Horiz.* **2016**, *3*, 208.
[24] Z. Ma, B. Su, S. Gong, Y. Wang, L. W. Yap, G. P. Simon, W. Cheng, *ACS Sens.* **2016**, *1*, 303.
[25] G. Y. Bae, S. W. Pak, D. Kim, G. Lee, D. H. Kim, Y. Chung, K. Cho, *Adv. Mater.* **2016**, *28*, 5300.
[26] X. Wang, Y. Gu, Z. Xiong, Z. Cui, T. Zhang, *Adv. Mater* **2014**, *26*, 1336.
[27] C. L. Choong, M. B. Shim, B. S. Lee, S. Jeon, D. S. Ko, T. H. Kang, J. Bae, S. H. Lee, K. E. Byun, J. Im, *Adv. Mater.* **2014**, *26*, 3451.
[28] A. A. Barlian, W.-T. Park, J. R. Mallon, A. J. Rastegar, B. L. Pruitt, *Proc. IEEE* **2009**, *97*, 513.
[29] W. Wu, X. Wen, Z. L. Wang, *Science* **2013**, *340*, 952.
[30] C. Dagdeviren, Y. Su, P. Joe, R. Yona, Y. Liu, Y.-S. Kim, Y. Huang, A. R. Damadoran, J. Xia, L. W. Martin, *Nat. Commun.* **2014**, *5*, 4496.
[31] M. H. Lee, H. R. Nicholls, *Mechatronics* **1999**, *9*, 1.
[32] T. Li, H. Luo, L. Qin, X. Wang, Z. Xiong, H. Ding, Y. Gu, Z. Liu, T. Zhang, *Small* **2016**, *12*, 5042.
[33] N. Jonassen, presented at *Electrical Overstress/Electrostatic Discharge Symposium Proceedings*, Reno, Nevada, USA, October **1998**.
[34] B. Nie, S. Xing, J. D. Brandt, T. Pan, *Lab Chip* **2012**, *12*, 1110.
[35] J. Y. Sun, C. Keplinger, G. M. Whitesides, Z. Suo, *Adv. Mater.* **2014**, *26*, 7608.
[36] B. Nie, R. Li, J. D. Brandt, T. Pan, *Lab Chip* **2014**, *14*, 1107.
[37] R. Li, B. Nie, P. Digiglio, T. Pan, *Adv. Funct. Mater.* **2014**, *24*, 6195.
[38] S. H. Cho, S. W. Lee, S. Yu, H. Kim, S. Chang, D. Kang, I. Hwang, H. S. Kang, B. Jeong, E. H. Kim, *ACS Appl. Mater. Interfaces* **2017**, *9*, 10128.
[39] M. J. Madou, *Fundamentals of Microfabrication: The Science of Miniaturization*, CRC Press, Boca Raton, USA **1997**.
[40] R. F. Turner, D. J. Harrison, R. V. Rojotte, *Biomaterials* **1991**, *12*, 361.
[41] G. Kim, H. Kim, I. Kim, J. Kim, J. Lee, M. Ree, *J. Biomater. Sci., Polym. Ed.* **2009**, *20*, 1687.
[42] L. Baxter, *Capacitive Sensors: Design and Applications*, Wiley-IEEE Press, Hoboken, USA **1996**.
[43] K. A. Mauritz, R. B. Moore, *Chem. Rev.* **2004**, *104*, 4535.
[44] G. Medrano, R. Bausch, A. Ismail, A. Cordes, R. Pikkemaat, S. Leonhardt, *J. Phys.: Conf. Ser.* **2010**, *224*, 012128.
[45] A. Michaels, S. Chandrasekaran, J. Shaw, *AIChE J.* **1975**, *21*, 985.
[46] E. McAdams, J. Jossinet, A. Lackermeier, F. Risacher, *Med. Biol. Eng. Comput.* **1996**, *34*, 397.
[47] H. Wang, L. Pilon, *J. Phys. Chem. C* **2011**, *115*, 16711.
[48] K. B. Oldham, *J. Electroanal. Chem.* **2008**, *613*, 131.
[49] O. Stern, *Z. Elektrochem.* **1924**, *30*, 1014.
[50] M. Kappl, *Surface and Interfacial Forces*, Wiley-VCH, Weinheim, Germany **2009**.
[51] Y. Sone, P. Ekdunge, D. Simonsson, *J. Electrochem. Soc.* **1996**, *143*, 1254.
[52] M. Born, E. Wolf, *Principles of Optics: Electromagnetic Theory of Propagation, Interference and Diffraction of Light*, 6th ed., Cambridge University Press, Cambridge, UK **1997**.
[53] S. P. Timoshenko, S. Woinowsky-Krieger, *Theory of Plates and Shells*, McGraw-Hill, New York, USA **1959**.
[54] G. Meng, W. H. Ko, *Sens. Actuators, A* **1999**, *75*, 45.
[55] Q. Wang, W. H. Ko, *Sens. Actuators, A* **1999**, *75*, 230.
[56] W. H. Ko, Q. Wang, *Sens. Actuators, A* **1999**, *75*, 242.

[57] J. C. Yeo, C. T. Lim, *Microsys. Nanoeng.* **2016**, *2*, 16043.
[58] R. Boyd, G. Smith, *Polymer Dynamics and Relaxation*, Cambridge University Press, Cambridge, UK **2007**.
[59] H. K. Iversen, T. Nielsen, J. Olesen, P. Tfelt-Hansen, *Lancet* **1990**, *336*, 837.
[60] M. J. Roman, T. G. Pickering, J. E. Schwartz, R. Pini, R. B. Devereux, *J. Am. Coll. Cardiol.* **1996**, *28*, 751.
[61] A. L. Pauca, S. L. Wallenhaupt, N. D. Kon, W. Y. Tucker, *Chest* **1992**, *102*, 1193.
[62] M. M. McDermott, M. H. Criqui, K. Liu, J. M. Guralnik, P. Greenland, G. J. Martin, W. Pearce, *J. Vasc. Surg.* **2000**, *32*, 1164.
[63] C. M. Boutry, A. Nguyen, Q. O. Lawal, A. Chortos, S. Rondeau-Gagné, Z. Bao, *Adv. Mater.* **2015**, *27*, 6954.
[64] D. G. Carey, L. A. Schwarz, G. J. Pliego, R. L. Raymond, *J. Sports Sci. Med.* **2005**, *4*, 482.
[65] A. L. Chesson Jr., R. A. Ferber, J. M. Fry, M. Grigg-Damberger, K. M. Hartse, T. D. Hurwitz, S. Johnson, G. A. Kader, M. Littner, G. Rosen, *Sleep* **1997**, *20*, 423.
[66] F. Q. AL-Khalidi, R. Saatchi, D. Burke, H. Elphick, S. Tan, *Pediatr. Pulm.* **2011**, *46*, 523.
[67] P.-G. Jung, G. Lim, S. Kim, K. Kong, *IEEE Trans. Ind. Inform.* **2015**, *11*, 485.
[68] R. Gurram, S. Rakheja, G. Gouw, *Ergonomics* **1995**, *38*, 684.
[69] J. Sanford, C. Young, D. Popa, N. Bugnariu, R. Patterson, presented at *SPIE Sensing Technology Applications*, Baltimore, Maryland, USA May **2014**.